Supporting Information for

Stimuli-Responsive Dimeric Capsule Built from Acridine-Based Metallacycle for Ratiometric Fluorescence Sensing of TNP

Qi-Qi Jin,[a, b,] Xiao-Fang Duan,[b] Dan-Ni Yan,[b] Fan Yin,[b, c] Chen-Chen Li,[b,c] Li-Peng Zhou,[b] Li-Xuan Cai*,[a, b, c] and Qing-Fu Sun*,[a, b, c]

[a] College of Chemistry and Materials Science, Fujian Normal University, Fuzhou 350007, P. R. China.

[b] State Key Laboratory of Structural Chemistry, Fujian Institute of Research on the Structure of Matter, Chinese Academy of Sciences, Fuzhou 350002, P. R. China.

[c] University of Chinese Academy of Sciences, Beijing, 100049, P. R. China.

*Correspondence to: lxcai@fjirsm.ac.cn; qfsun@fjirsm.ac.cn

Table of Content

1. Supplemental spectra of **L** and **1**
2. Single crystal X-ray diffraction study
3. Calculation of K_a
4. Photophysical properties of **1**
5. Sensing of **TNP** and other nitro-compounds
6. Supplementary reference

1. Synthesis and self-assembly of L

L was synthesized according to the previous literature [S1].

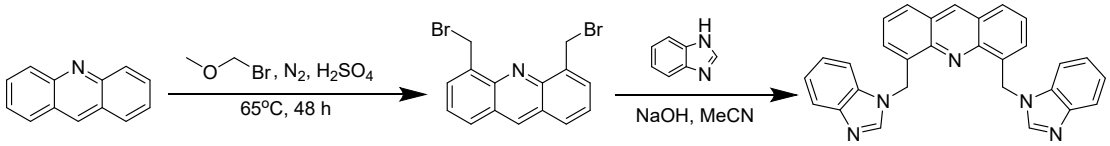

Scheme S1. Synthesis of **L**.

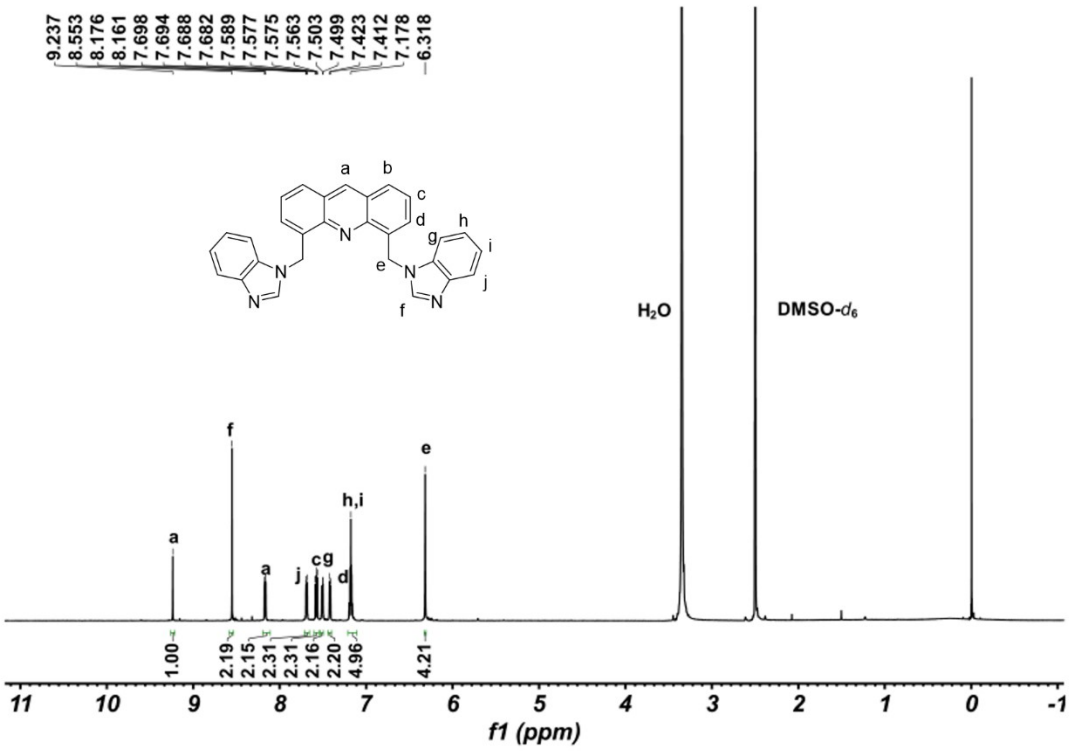

Figure S1. ^{1}H NMR spectrum (400 MHz, DMSO-d_6, 298 K) of **L**.

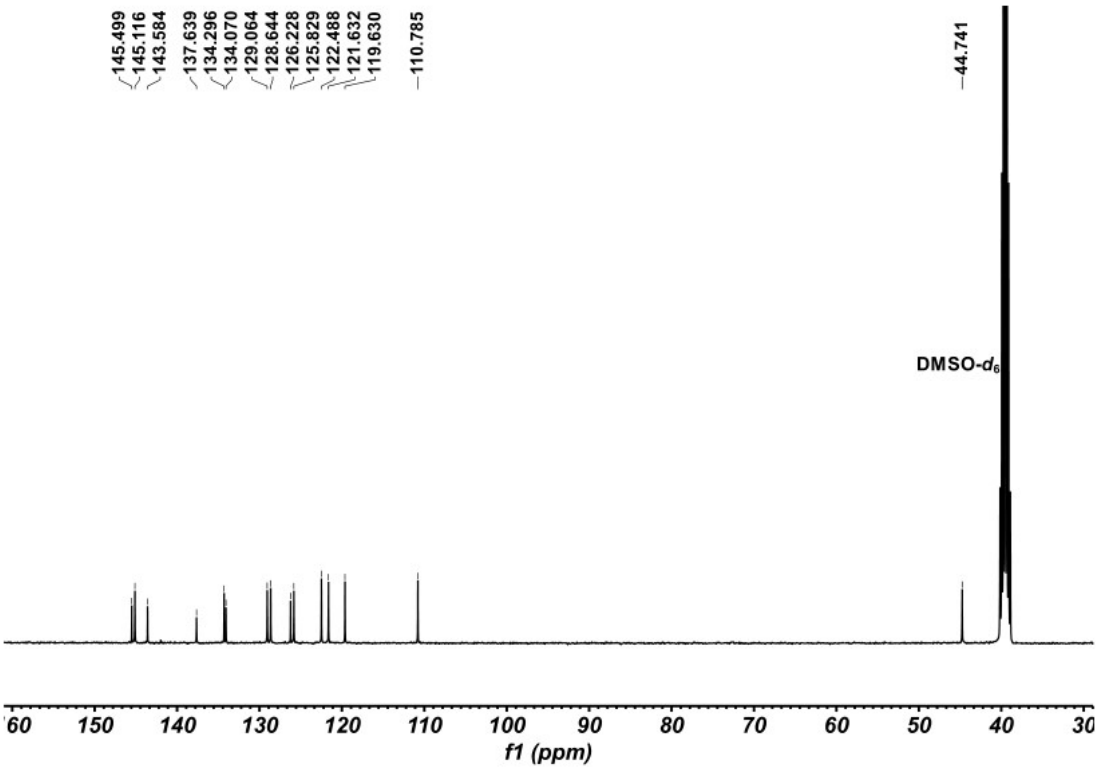

Figure S2. ^{13}C NMR spectrum (151 MHz, DMSO-d_6, 298 K) of **L**.

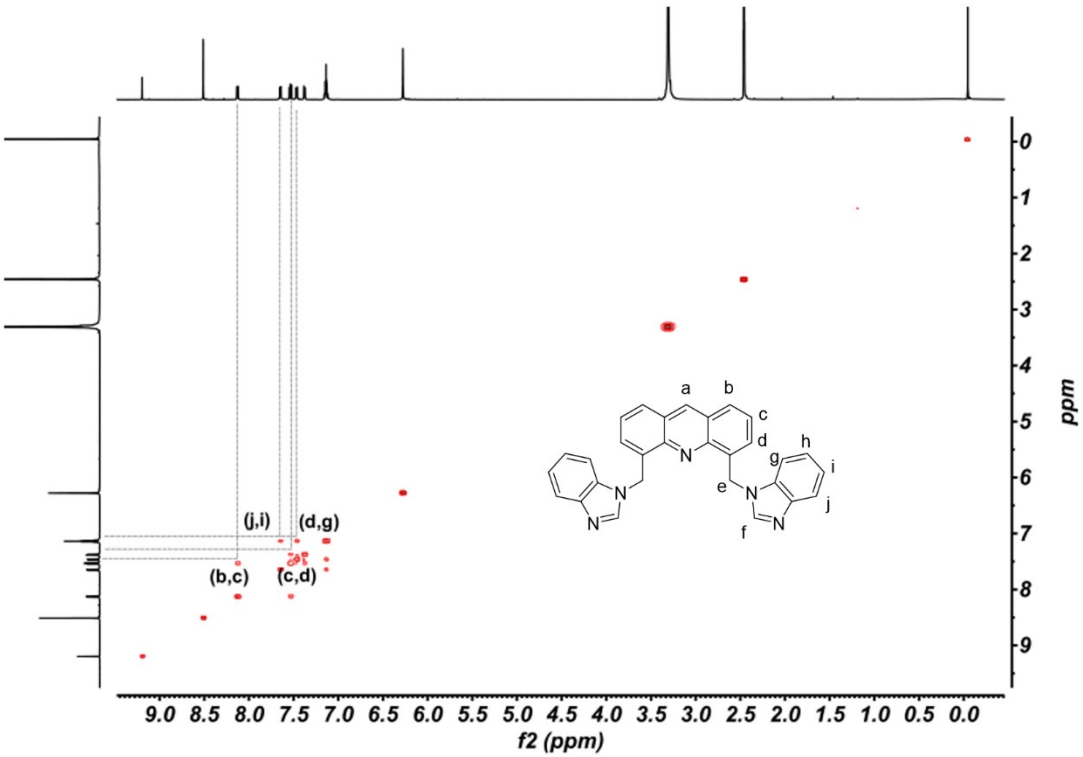

Figure S3. ^{1}H-^{1}H COSY NMR spectrum (400 MHz, DMSO-d_6, 298 K) of **L**.

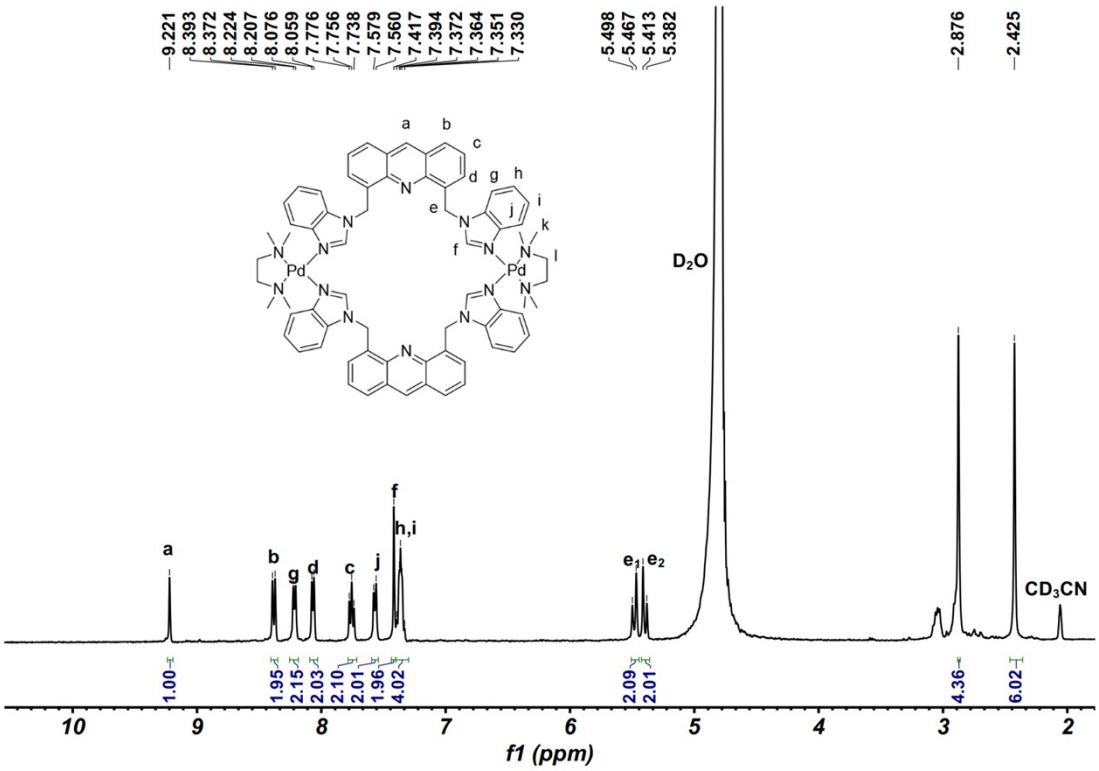

Figure S4. ^{1}H NMR spectrum (400 MHz, D_2O/CD_3CN, v/v = 19/1,298 K) of the self-assembly of L and tmedPd$(NO_3)_2$.

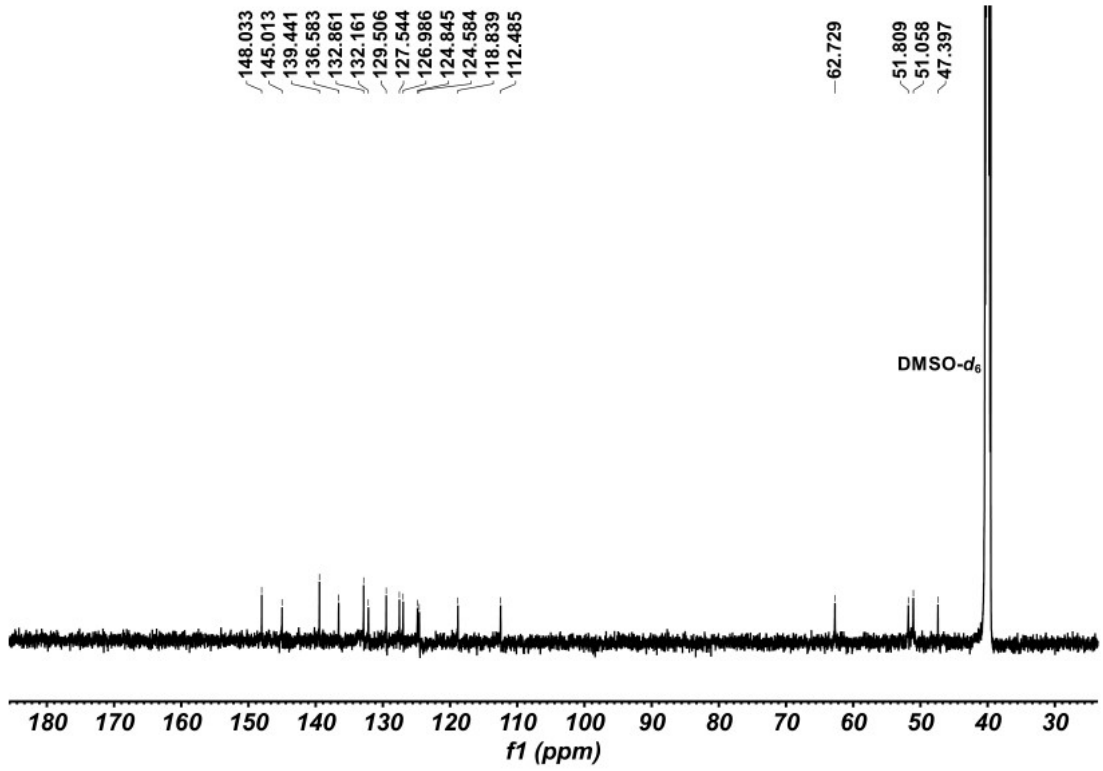

Figure S5. ^{13}C NMR spectrum (151 MHz, DMSO-d_6, 298 K) of the self-assembly of L and tmedPd$(NO_3)_2$.

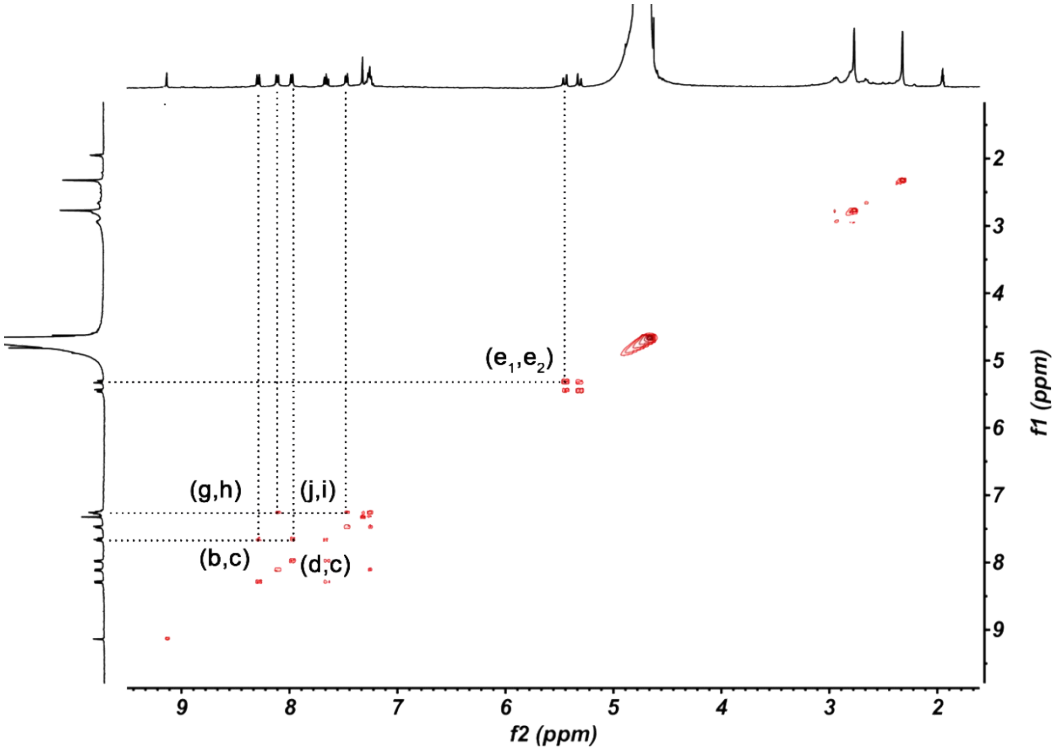

Figure S6. ^{1}H-^{1}H COSY NMR spectrum (400 MHz, D_2O/CD_3CN, v/v = 19/1, 298 K) of the self-assembly of L and tmedPd$(NO_3)_2$.

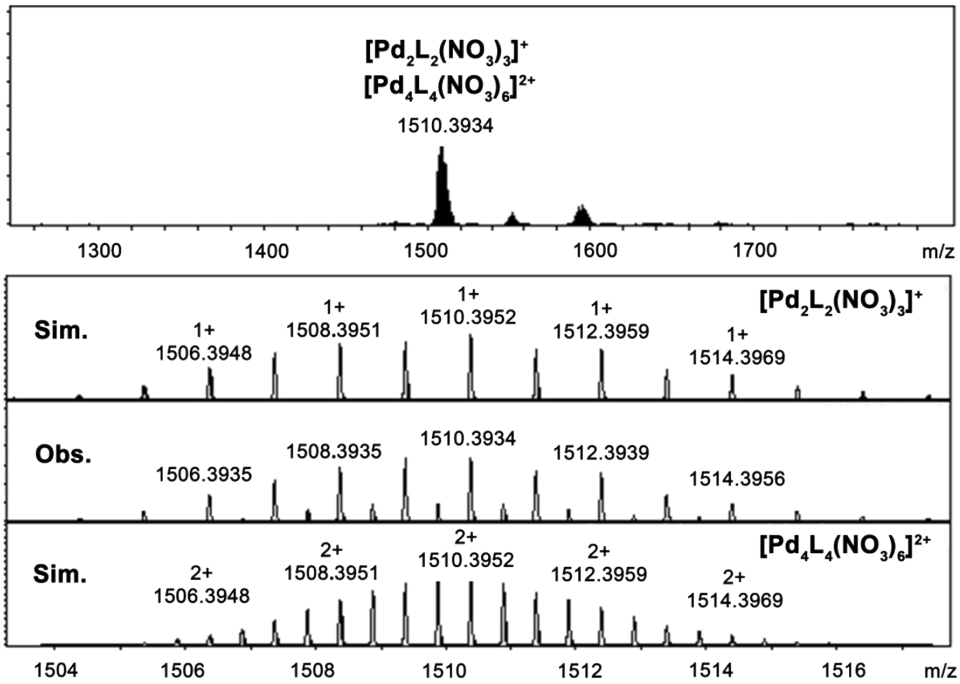

Figure S7. ESI-TOF-MS of the monomer and dimer mixture.

We used Bruker TopSpin 4.0.6 software for precise data fitting, and determined the diffusion coefficients based on intensities as a function of the diffusion delay time. The average diffusion coefficients (D values) obtained are 2.33×10^{-10} m^2s^{-1} (c = 2.5 mM) for **1** in D_2O/CD_3CN (v/v = 19/1), and 9.00×10^{-10} m^2s^{-1} for **1** in CD_3CN. The fitted decay curves and the ^{1}H DOSY spectra are shown in Figures S8-S9.

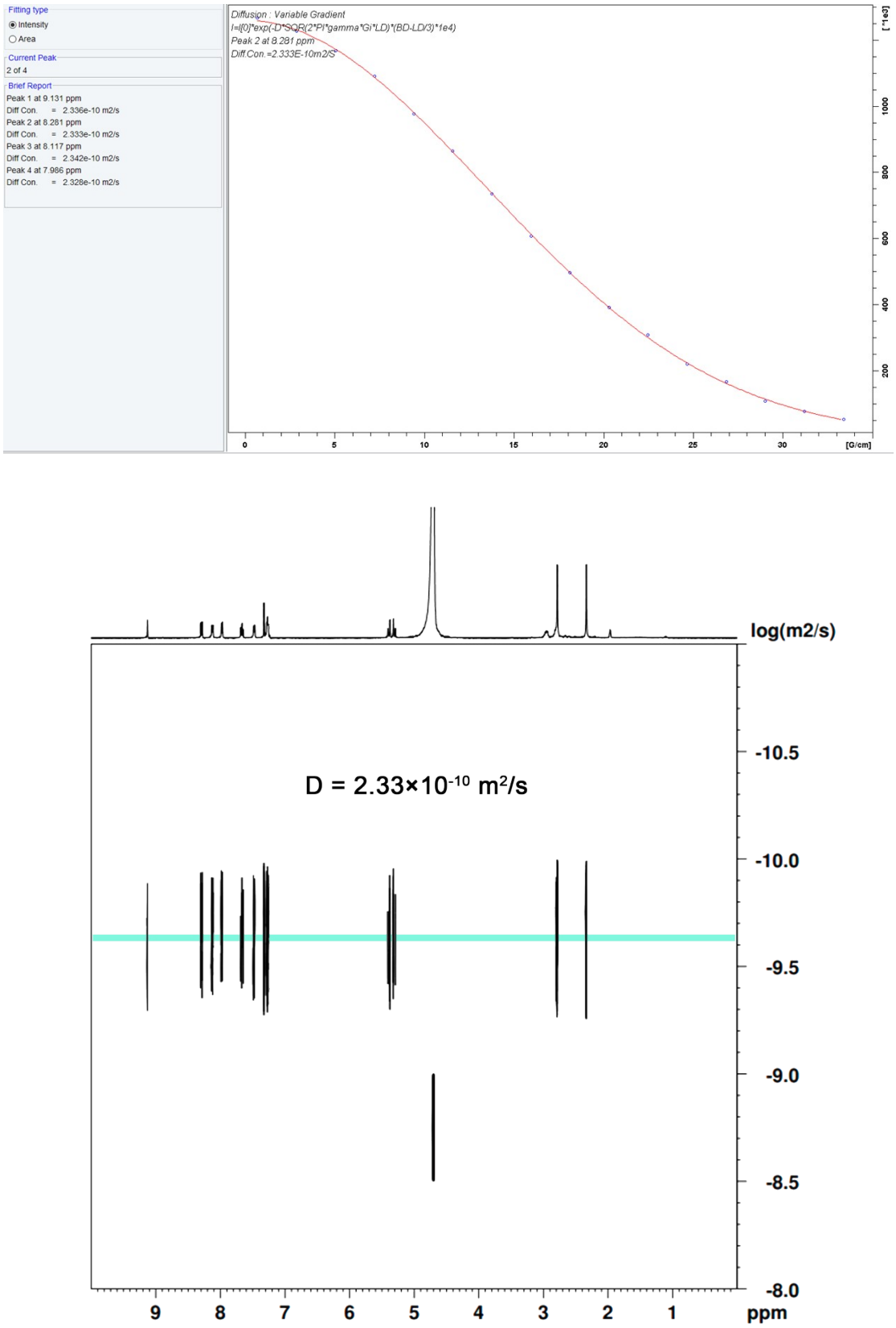

Figure S8. ^{1}H DOSY spectrum of **1** (400 MHz, 298 K, D_2O/CD_3CN, v/v = 19/1, c = 2.5 mM, Diffusion Coefficient D = 2.33×10^{-10} m^2s^{-1}, d = 1.85 nm).

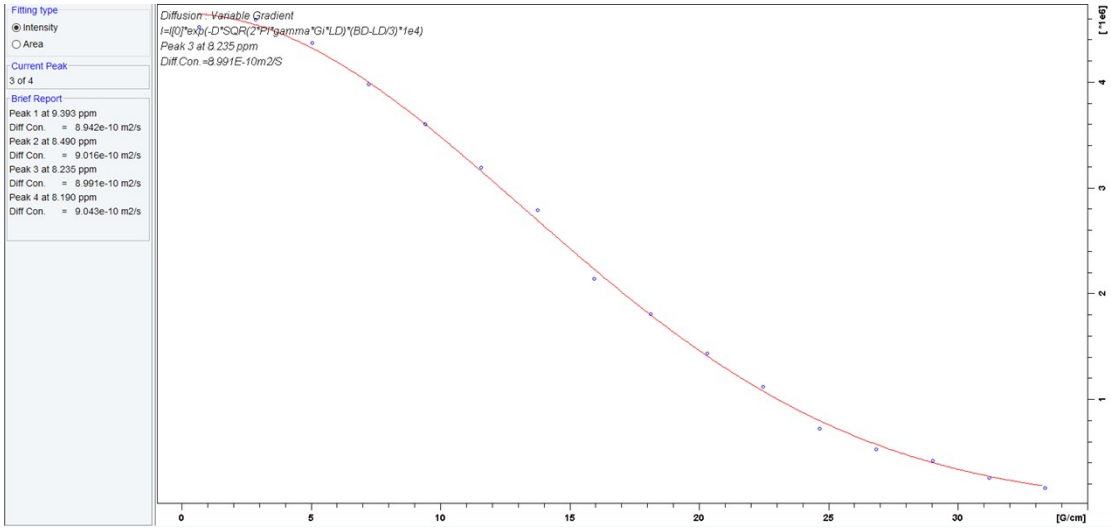

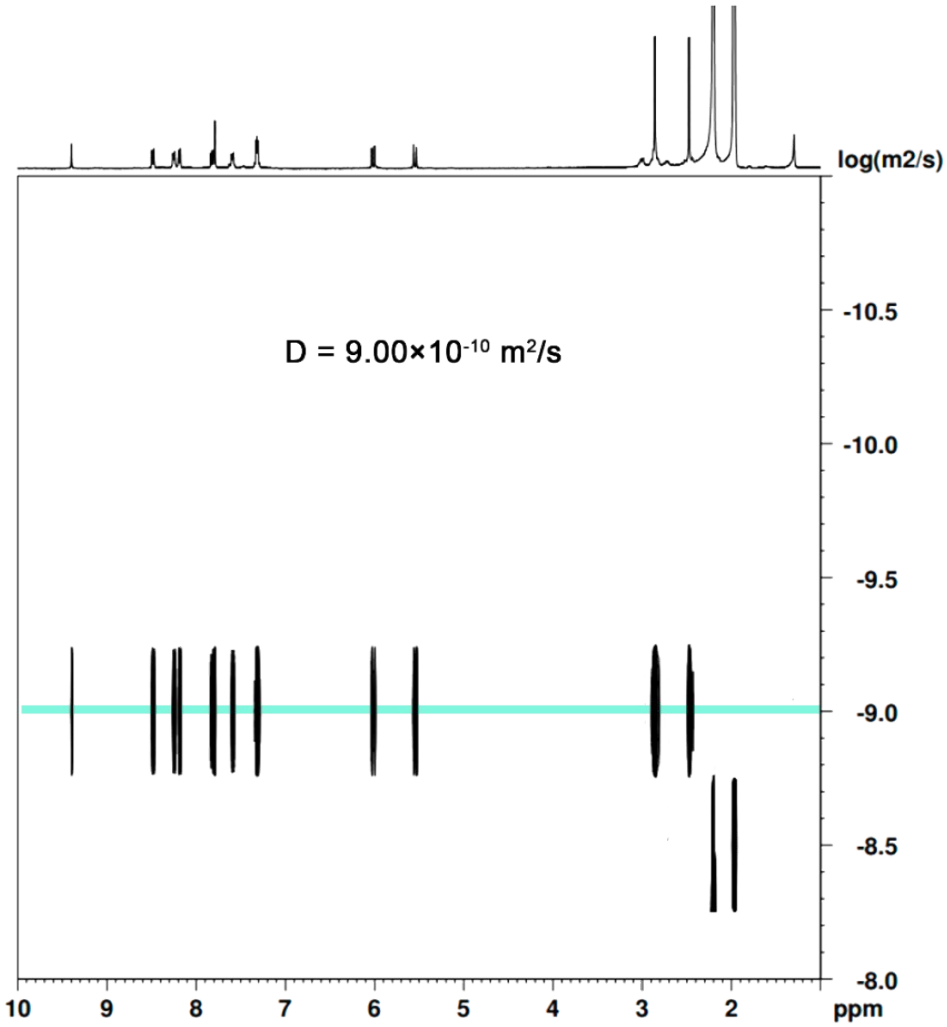

Figure S9. ^{1}H DOSY spectrum of **1** (400 MHz, 298 K, CD_3CN, c = 1 mM, Diffusion Coefficient D = 9.00×10^{-10} m^2s^{-1}, d = 1.24 nm).

2. Single crystal X-ray diffraction study:

X-ray diffraction study for **1** was conducted at a Rigaku XtaLAB Synergy R diffractometer using MoKα radiation (λ = 0.71073 Å). Data reduction was performed with the CrysAlisPro package.[S2] Subsequently, the structures were solved through the direct method and refined using full-matrix least-squares on F_2 with consideration of anisotropic displacement, employing the SHELX software package.[S3] Solvent molecules were highly disordered and could not be reasonably located. PLATON/SQUEEZE routine[S4] was used to remove the contribution of the electron density associated with the remaining highly disordered solvents. Thermal parameter restraints (SIMU, DELU) were applied to the framework to obtain the chemical-reasonable models and reasonable atomic displacement parameters. OMIT restraint was also used to delete two reflections with large Error/esd values.

Crystal data for **1**: Space group *P*-1, a = 17.1274(2) Å, b = 17.2676(3) Å, c = 19.2750(3) Å, V = 4850.30(15) Å^3, Z = 2, T = 100(2) K. Anisotropic least-squares refinement on 19463 independent merged reflections (R_{int} = 0.0494) converged at residual ${}_wR_2$ = 0.2256 for all data; residual R_1 = 0.0592 for 15546 observed data [I > 2σ (I)], and goodness of fit (GOF) =0.933. (CCDC 2404246)

Note: PLATON/SQUEEZE routine gave a total potential solvent accessible void of 1827 Å^3 per unit cell and a total of approximately 590 electron count. Due to the presence of three possible disordered solvents in the crystal (water, DMSO, and THF), the identity of the masked solvents could not be conclusively determined. These molecules have not been included in the molecular formula. As a result, the reported molecular weight and density are underestimated.

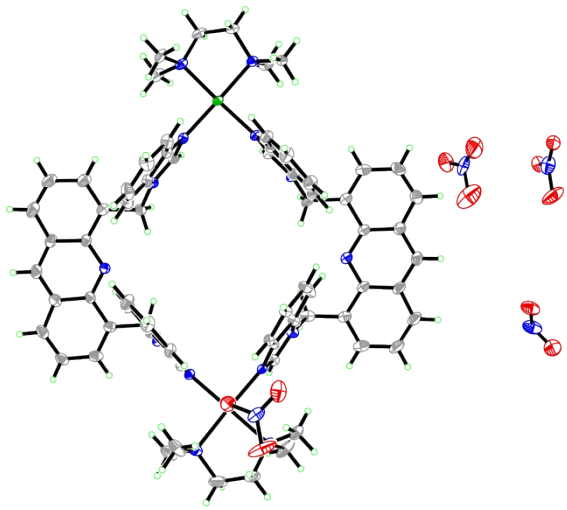

Figure S10. Ortep drawing of the asymmetric unit in the crystal structure of **1** at 30% probability level.

Table S1. Crystal data and structure refinement for **1**.

Identification code	jqq-230318_auto_sq
Empirical formula	$C_{70}H_{74}N_{18}O_{12}Pd_2$
Formula weight	1572.27
Temperature	100(2) K
Wavelength	0.71073 Å
Crystal system	Triclinic
Space group	*P*-1
Unit cell dimensions	a = 17.1274(2) Å
	b = 17.2676(3) Å
	c = 19.2750(3) Å
Volume	4850.30(15) Å3
Z	2
Density (calculated)	1.077 Mg/m^3
Absorption coefficient	0.425 mm^{-1}
F(000)	1616
Crystal size	0.2 x 0.18 x 0.15 mm^3
Theta range for data collection	1.537 to 28.342°.
Index ranges	-22<=h<=21, -22<=k<=22, -24<=l<=24
Reflections collected	78239
Independent reflections	19463 [R(int) = 0.0494]
Completeness to theta = 25.242°	98.4 %
Refinement method	Full-matrix least-squares on F^2
Data / restraints / parameters	19463 / 1694 / 927
Goodness-of-fit on F2	0.933
Final R indices [I>2sigma(I)]	R1 = 0.0592, wR2 = 0.2113
R indices (all data)	R1 = 0.0742, wR2 = 0.2256
Extinction coefficient	1.943 and -1.019 e.$Å^{-3}$

3. Weak Interaction Analysis

The independent gradient model (IGM) analysis was conducted using the Multiwfn 3.8 program to explore the weak interactions between the host and NO_3^-. During the calculation process, the host–guest complex is split into two fragments (the host and guest NO_3^-) to study their interactions. The contribution degree of atomic pair and atoms to the weak interaction is quantified as a percentage using the δg index. The molecular structure diagram, depicting the color-coded atomic δg index and δg_{inter} isosurface, was generated using the VMD 1.9.3 program. The color scale, ranging from red to orange (-0.8 to 0.2), effectively visualizes the δg index variations among different atoms. The smaller value of δg_{inter} isosurface is set to ensure the ideal visualization of the *vdw* between the host and guest."

Figure S11. Color-coded sign scale bar of IGM analysis.

4. Calculation of K_a:

Since the process of monomer dimerization is actually a fast exchange process, we adopted the Hill equation[S5] for fitting to calculate the dimerization constant. The details are modified as follows:

$$1 + 1' \rightleftharpoons (1)_2$$

$$\log \frac{\theta_i}{1-\theta_i} = n\log[\Delta 1] + n\log[K_a]$$

$$\theta_i = \frac{\Delta\delta_i}{\Delta\delta_{max}}$$

$$n = Hill\ coefficient$$

$$[1'] = [1] - [1]_0$$

$$K_\alpha = dimerization\ constant$$

Where the value of θ_i was obtained by using $\Delta\delta_i$ as compared against the maximum change of chemical shift $\Delta\delta_{max}$ of H_a in ^1H NMR spectra, n is the Hill coefficient describing cooperativity, and K_a is the apparent dimerization constant. The Hill coefficient n describes the cooperative binding, where $n > 1$ indicates positive cooperativity, $n < 1$ indicates negative cooperativity, and $n = 1$ indicates no cooperativity.

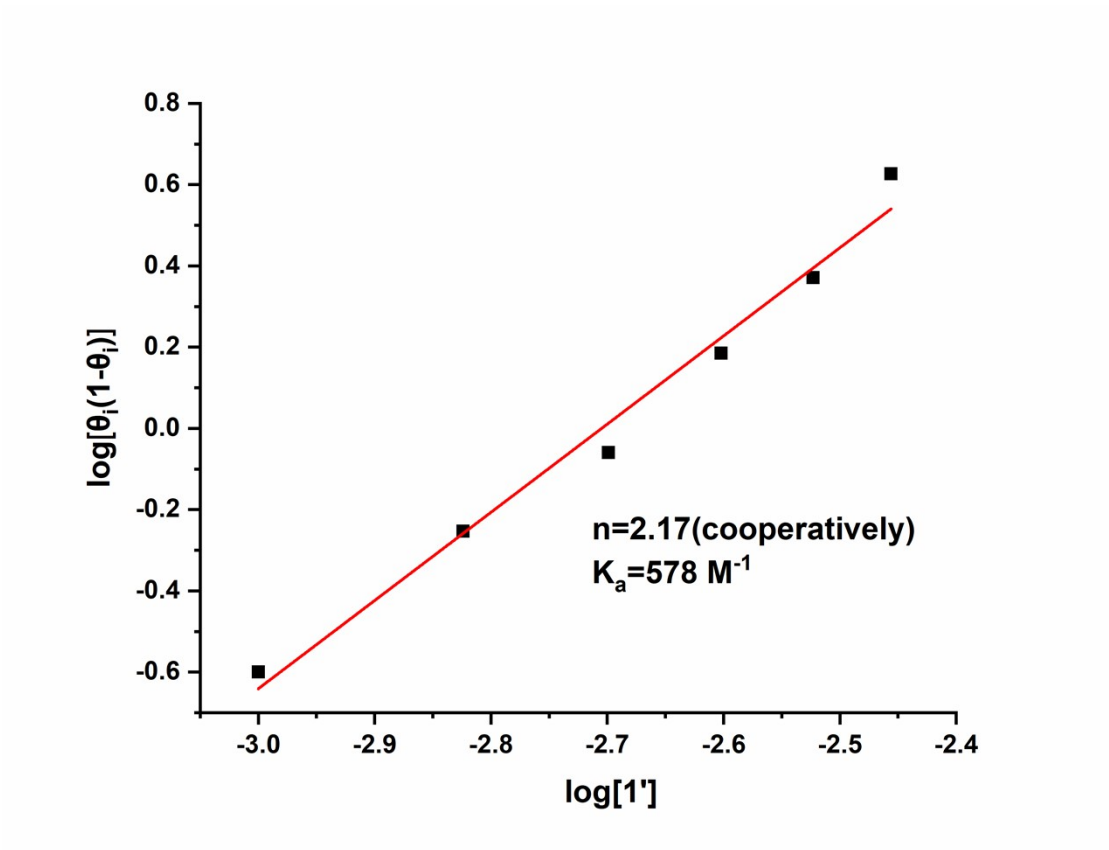

Figure S12. Titration curve fitting with Hill function for different concentrations in CD_3CN.

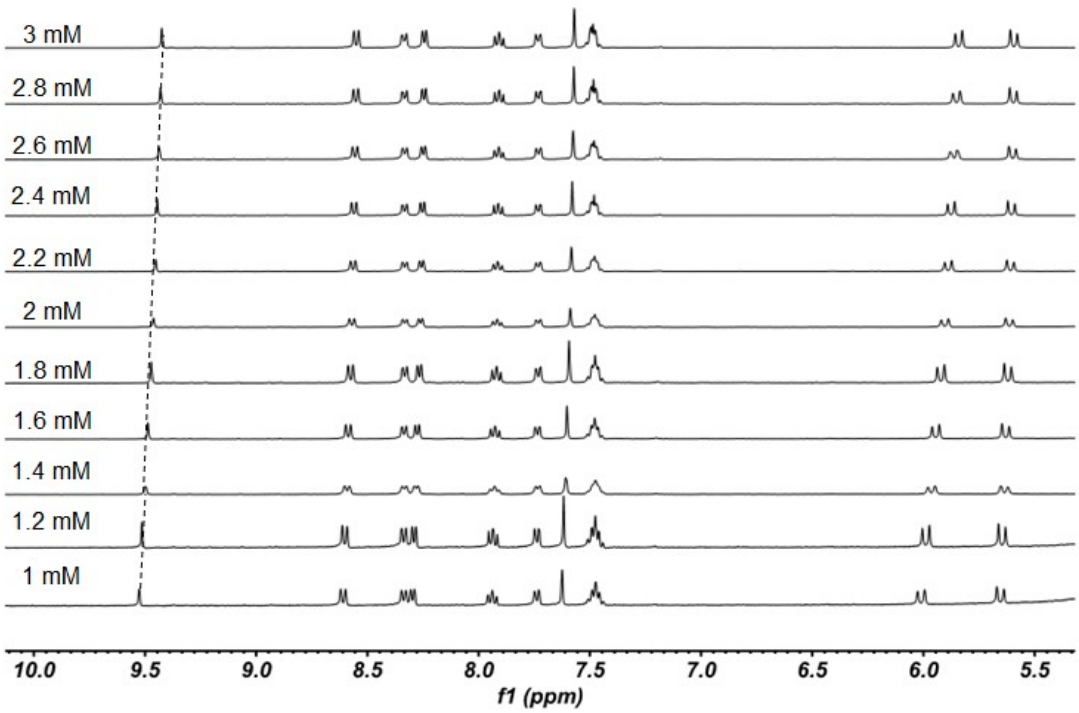

Figure S13. ^{1}H NMR titration (400 MHz, D_2O/CD_3CN, v/v = 4/1, 298 K) of **1** with different concentrations.

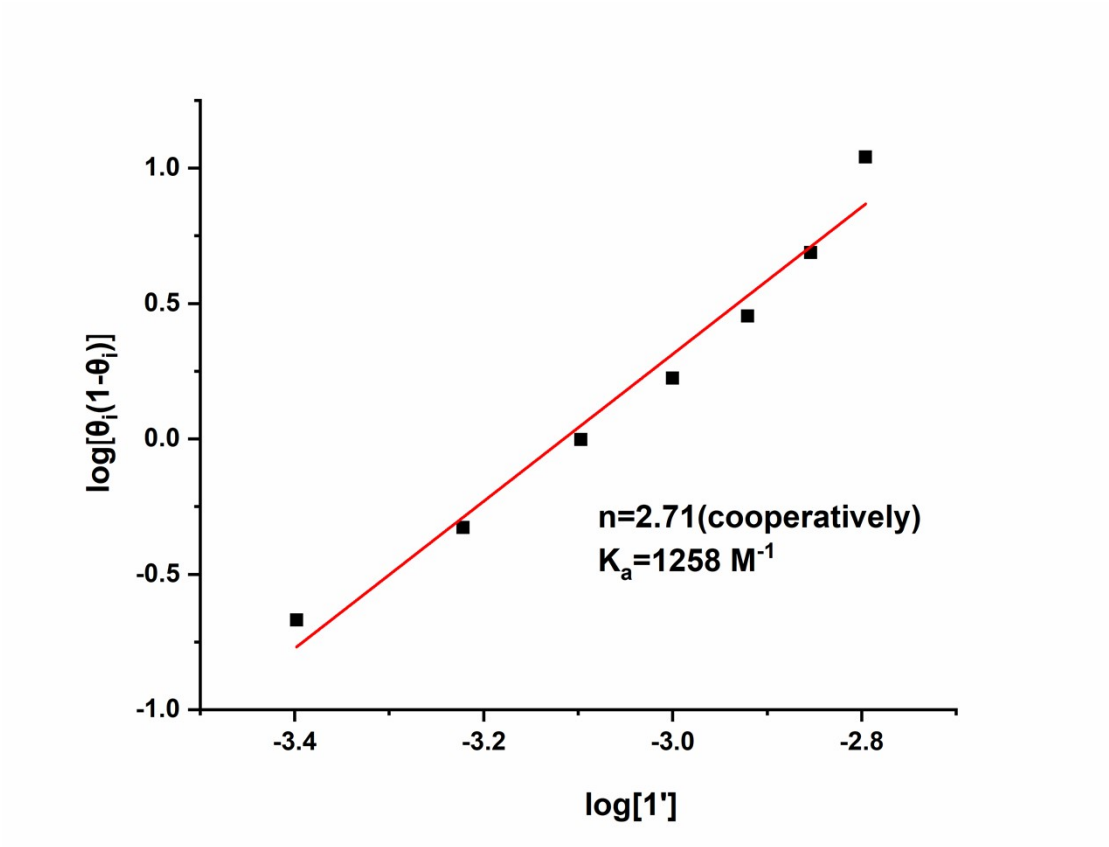

Figure S14. Titration curve fitting with Hill function for different concentrations in a mixture of D_2O and CD_3CN (D_2O/CD_3CN, v/v = 4/1).

4. Photophysical properties of 1:

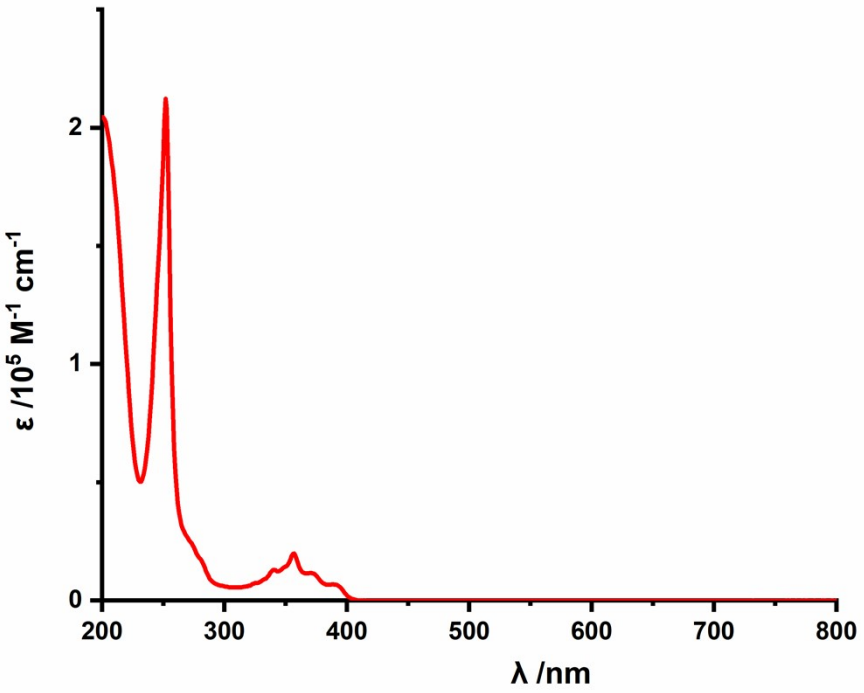

Figure S15. UV-Vis spectrum of **1** in CH_3CN (0.01 mM).

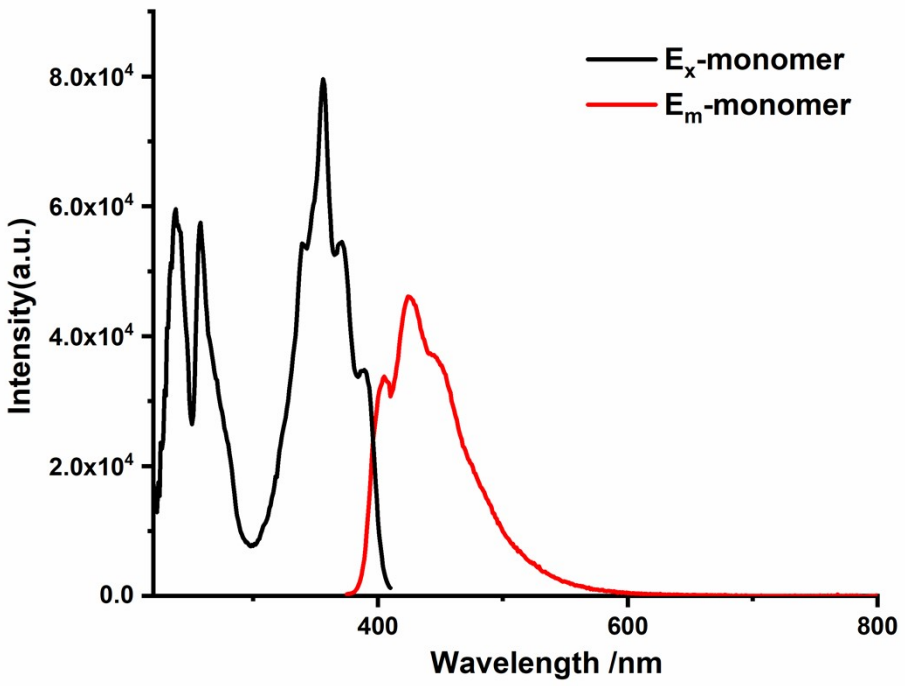

Figure S16. Fluorescence excitation and emission spectra of **1** in CH_3CN (λ_{ex} = 357 nm, λ_{em} = 430 nm, 0.01 mM, slits: 3.0 - 2.0).

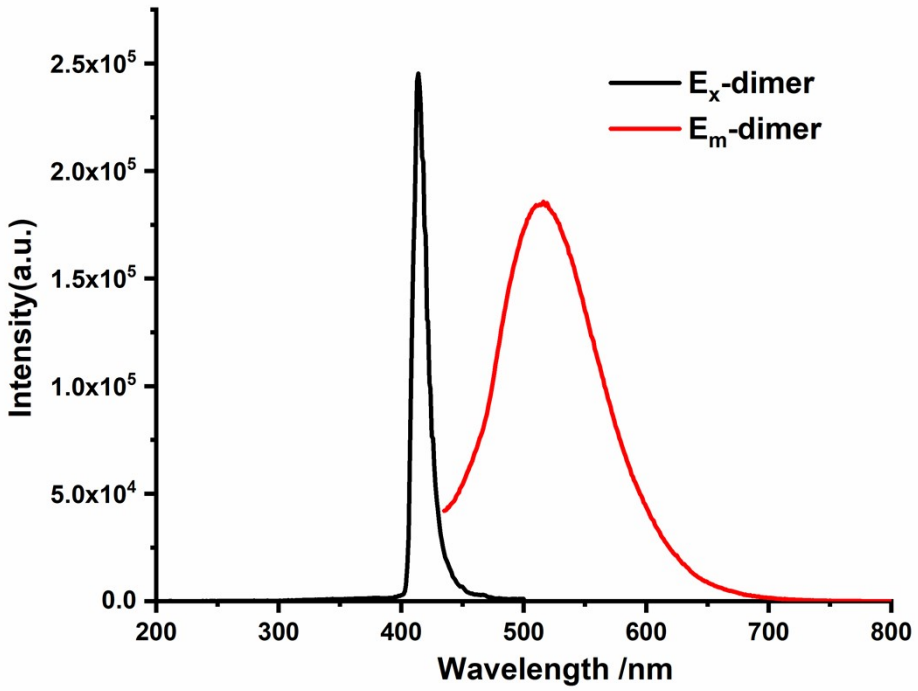

Figure S17. Fluorescence excitation and emission spectra of $(\mathbf{1})_2$ in H_2O/CH_3CN (v/v = 19/1) (λ_{ex} = 414 nm, λ_{em} = 520 nm, 5 mM, slits: 3.0 - 2.0).

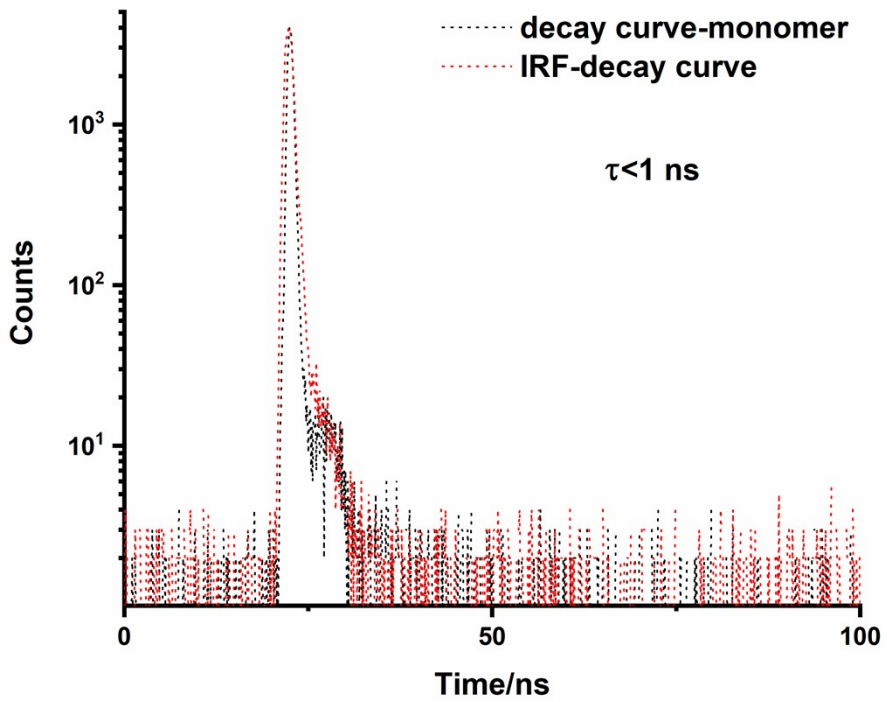

Figure S18. Fluorescence decay curve of **1** in H_2O/CH_3CN (v/v = 4/1) (λ_{ex} = 375 nm, λ_{em} = 430 nm, 1 mM).

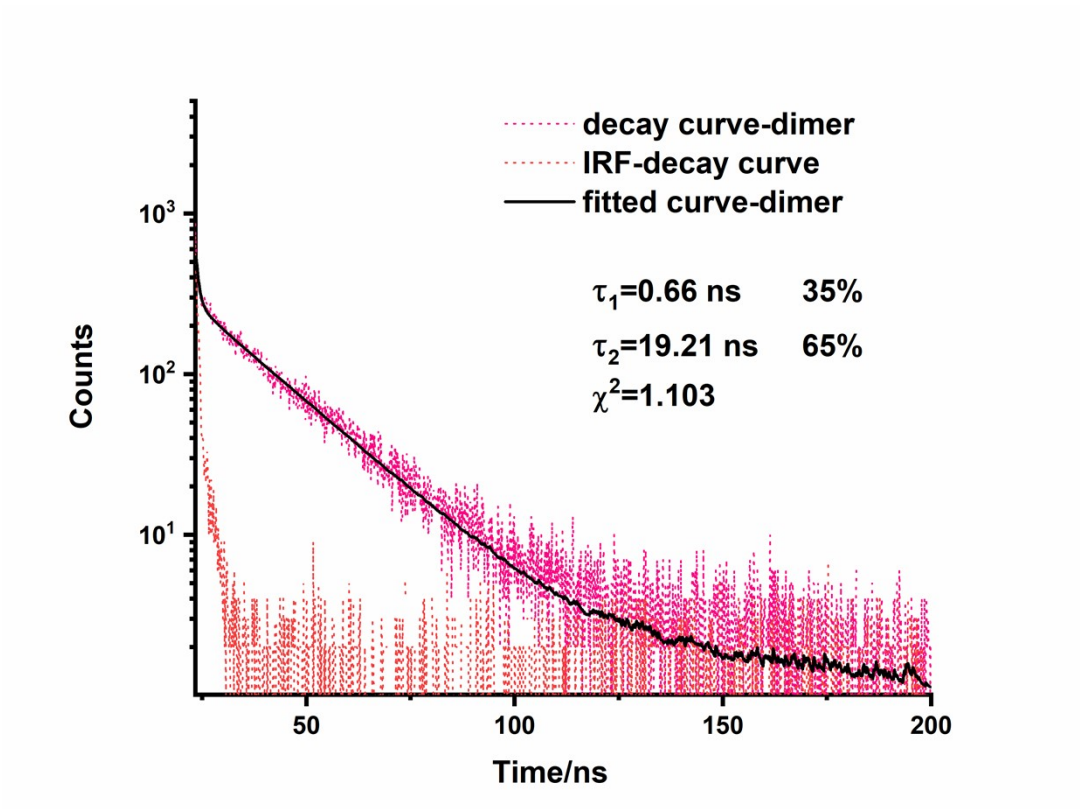

Figure S19. Fluorescence decay and fitted curves of **1** in H_2O/CH_3CN (v/v = 19/1) (λ_{ex} = 375 nm, λ_{em} = 520 nm, 1 mM).

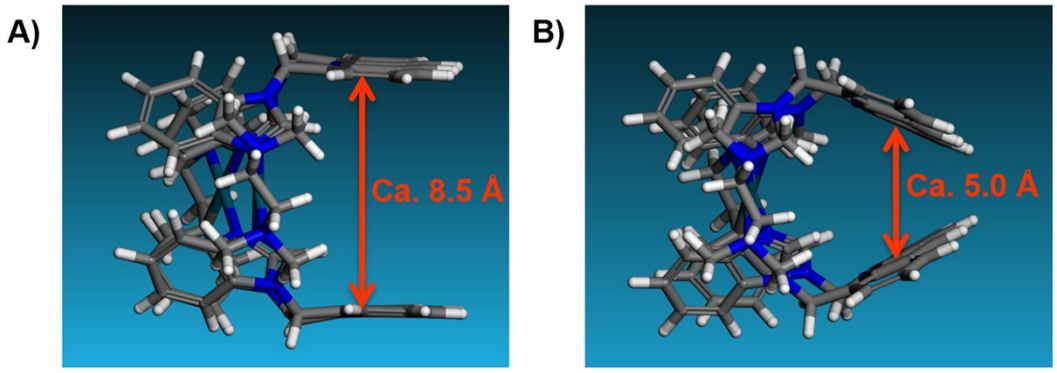

Figure S20. Simulated structures of another conformation of **1** under the conditions A) before optimization and B) after optimization.

5. Sensing of TNP and other nitro-compounds

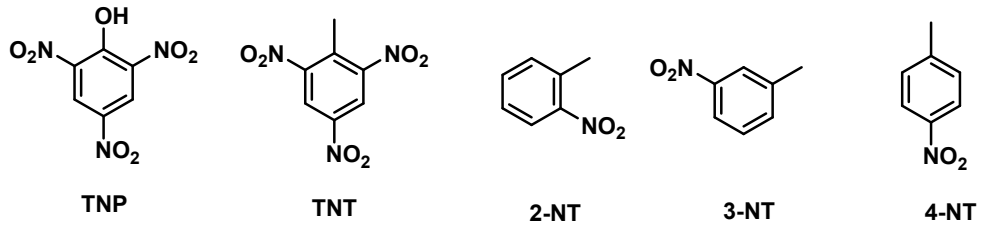

Figure S21. Chemical structures of commonly considered explosive nitro-aromatic compounds.

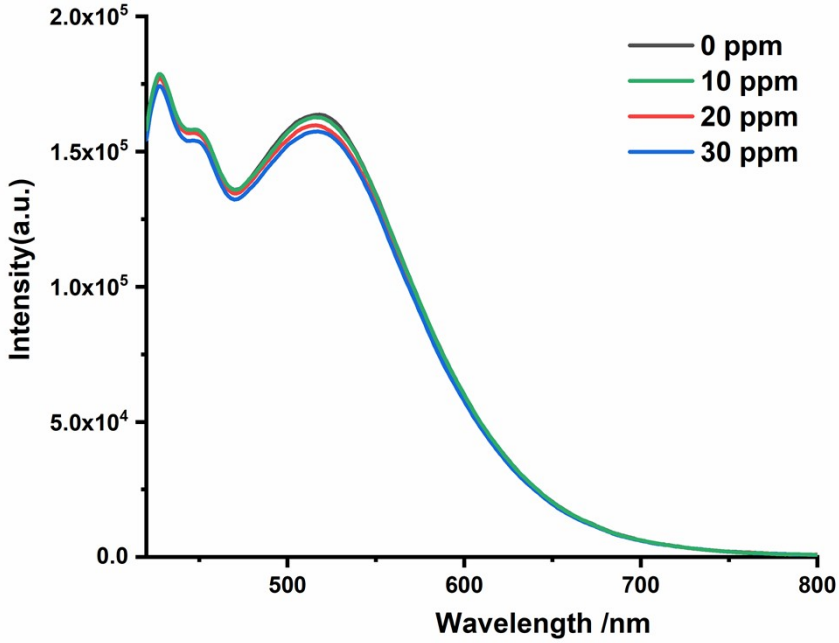

Figure S22. Fluorescence emission spectra of **1** in a mixture of H_2O and CH_3CN (v/v = 4/1) (λ_{ex} = 405 nm, 1 mM, slits: 3.0 - 2.0) with increasing concentrations of **TNT**.

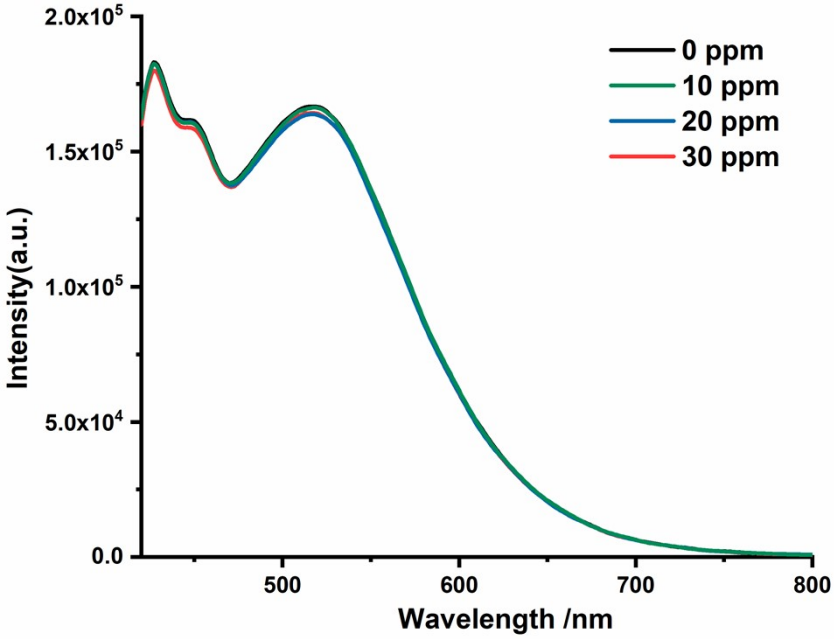

Figure S23. Fluorescence emission spectra of **1** in a mixture of H_2O and CH_3CN (v/v = 4/1) (λ_{ex} = 405 nm, 1 mM, slits: 3.0 - 2.0) with increasing concentrations of **2-NT**.

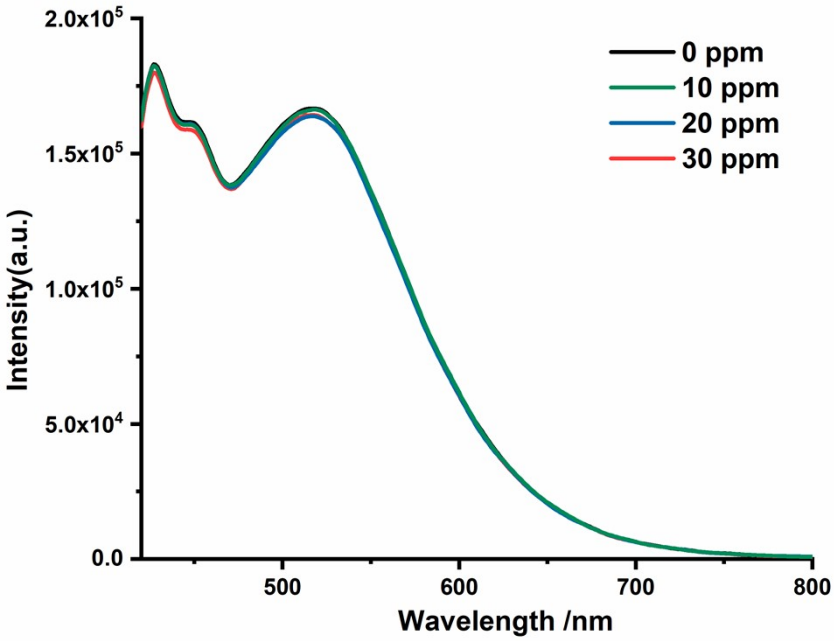

Figure S24. Fluorescence emission spectra of **1** in a mixture of H_2O and CH_3CN (v/v = 4/1) (λ_{ex} = 405 nm, 1 mM, slits: 3.0 - 2.0) with increasing concentrations of **3-NT**.

Figure S25. Fluorescence emission spectra of **1** in a mixture of H_2O and CH_3CN (v/v = 4/1) (λ_{ex} = 405 nm, 1 mM, slits: 3.0 - 2.0) with increasing concentrations of **4-NT**.

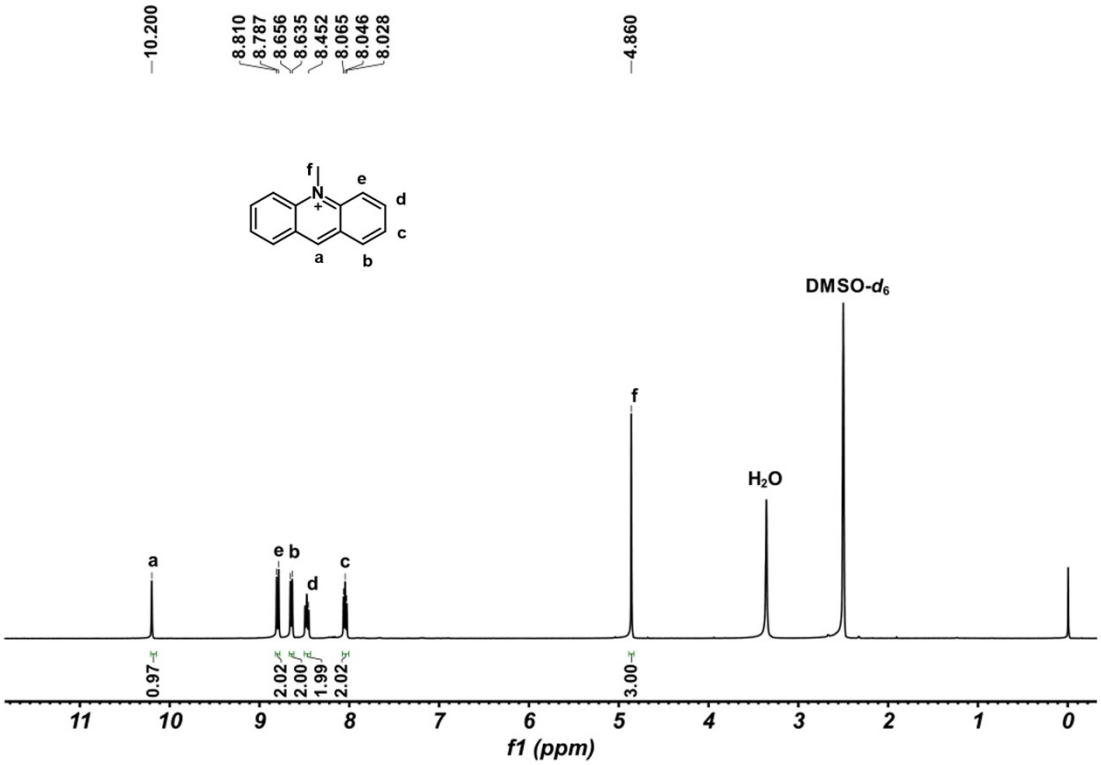

Figure S26. ^{1}H NMR spectrum (400 MHz, DMSO-d_6, 298 K) of N-methylacridine.

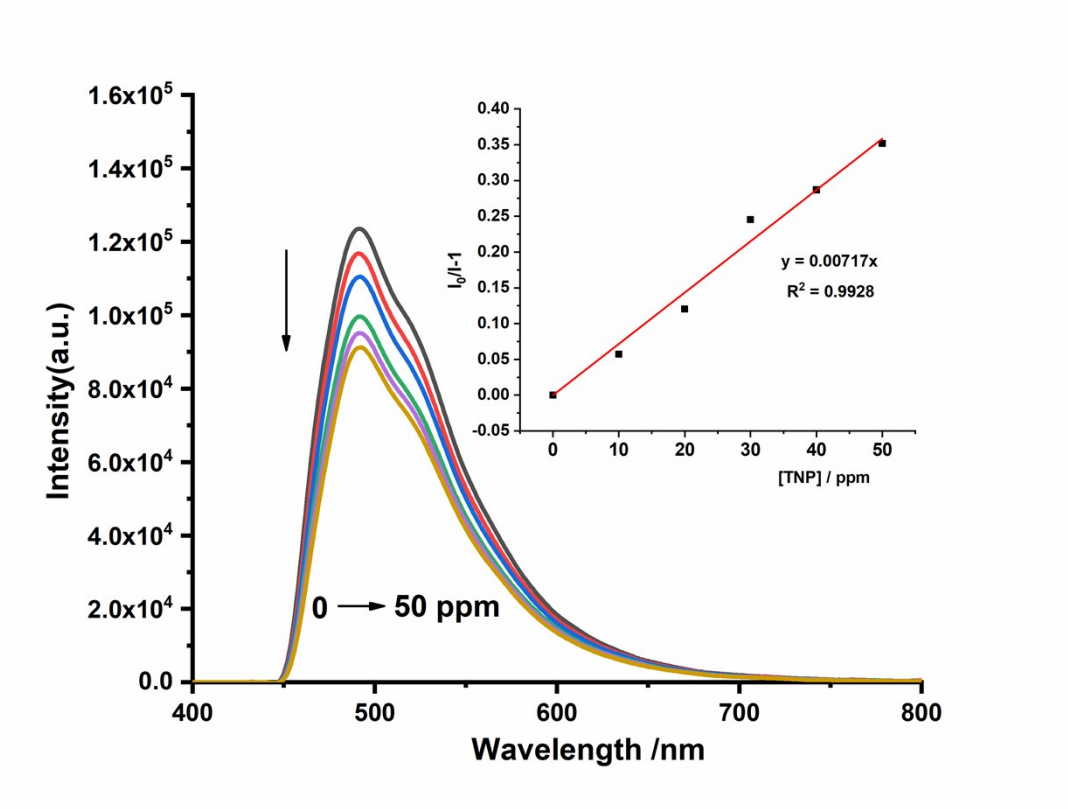

Figure S27. Fluorescence emission spectra of N-methylacridine with varying concentrations of TNP (0-50 ppm) in a mixture of H_2O and CH_3CN (v/v = 4/1) (c = 2.0 mM, λ_{ex} = 363 nm). Inset: The S-V plot of fluorescence intensity (I_0/I - 1) versus TNP concentration, ranging from 0 to 50 ppm.

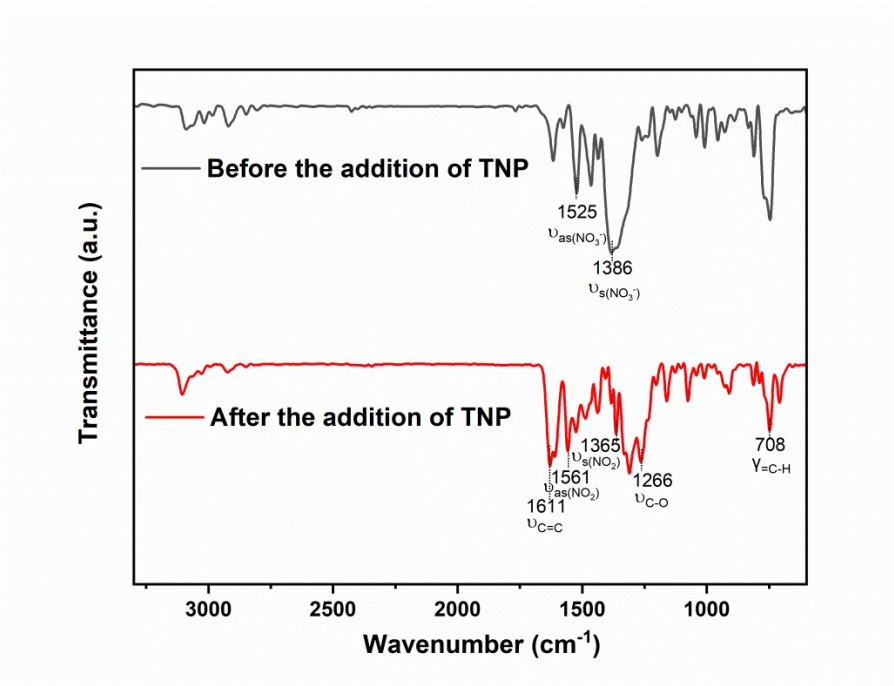

Figure S28. IR spectra of the complex before and after the addition of TNP.

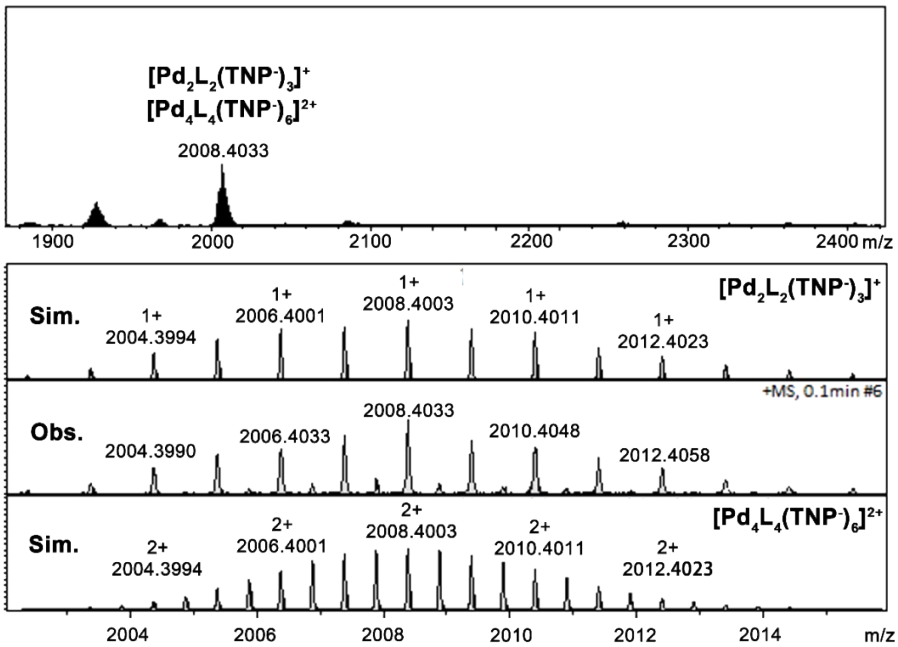

Figure S29. ESI-MS spectra of the complex after the addition of TNP.

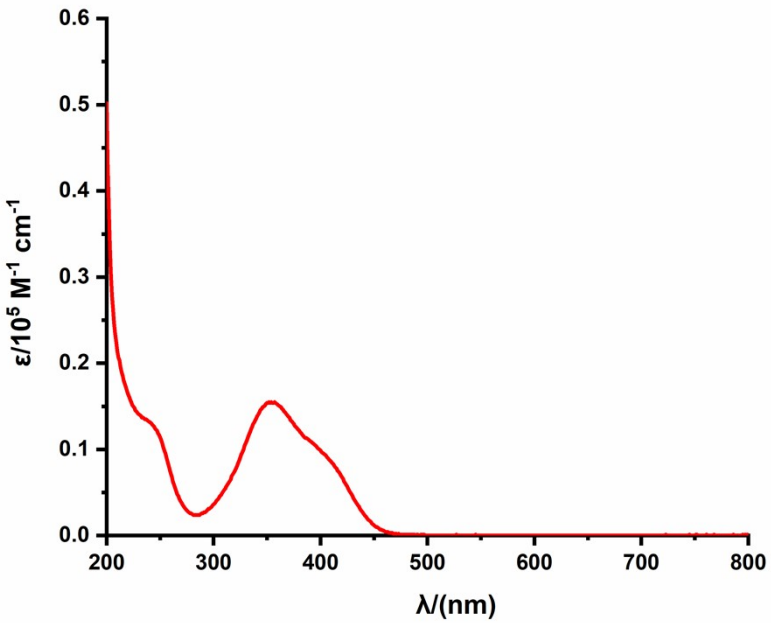

Figure S30. UV-Vis spectra of TNP.

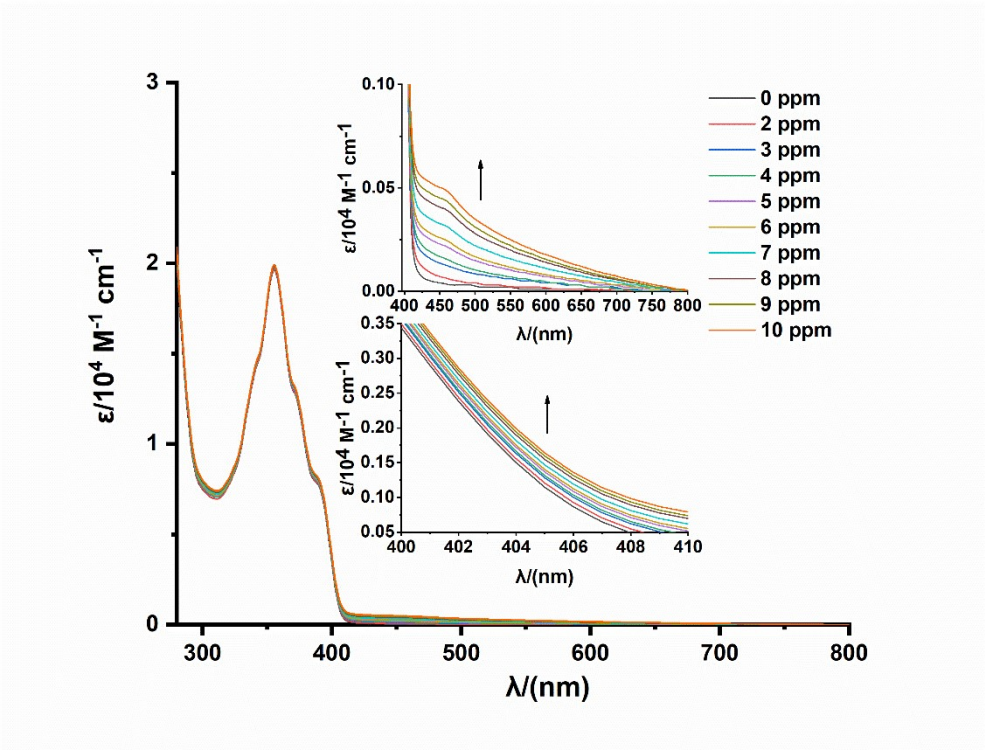

Figure S31. UV-Vis titration of **1** (1 mM) with 1-10 ppm of TNP.

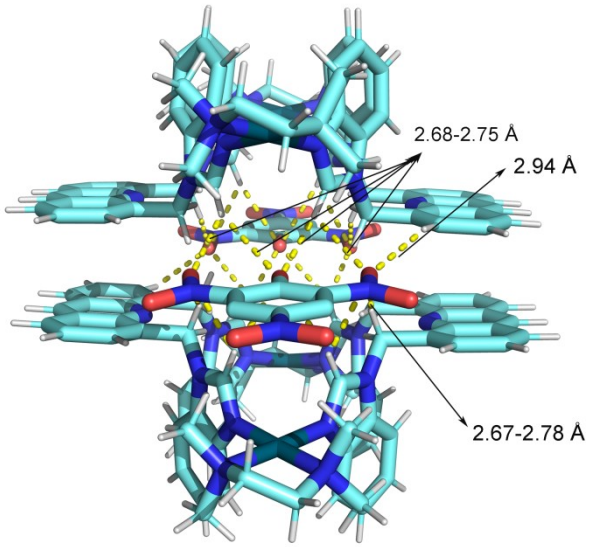

Figure S32. Simulated structure of **1** with TNP. Multiple hydrogen bonds mainly formed between benzimidazolium C-H and nitro group and hydroxyl anion of TNP^-.

6. Supplementary reference:

[S1]. *Synthesis*, 2010, **3**, 465–469.
[S2]. Agilent Technologies,CrysAlisPro v. 1.171.36.28, 2013.
[S3]. G. M., Sheldrick , Acta Crystallogr. Sect. A, 2008, **64**, 112-122.
[S4]. A. L., Spek, J. Appl. Crystallogr., 2003, **36**, 7-13.
[S5]. (a) Takezawa, H.; Murase, T.; Resnati, G.; Metrangolo, P.; Fujita, M., *J. Am. Chem. Soc.* 2014, **136**, 1786-1788. (b) Yang, D.; Greenfield, J. L.; Ronson, T. K.; von Krbek, L. K. S.; Yu, L.; Nitschke, J. R., *J. Am. Chem. Soc.* 2020, **142**, 19856-19861. (c) Li, K.; Wu, K.; Lu, Y.-L.; Guo, J.; Hu, P.; Su, C.-Y., *Angew. Chem. Int. Ed.*, 2022, **61**, e202114070.